Electrochimica Acta 62 (2012) 163–171

Contents lists available at SciVerse ScienceDirect

Electrochimica Acta

journal homepage: www.elsevier.com/locate/electacta

Influence of size and oxidative treatments of multi-walled carbon nanotubes on their electrocatalytic properties

Paulina Cañete-Rosales[a], Valeria Ortega[a], Alejandro Álvarez-Lueje[a], Soledad Bollo[a,*,1], Mónica González[b], Alejandro Ansón[b], María Teresa Martínez[b]

[a] Departamento de Química Farmacológica y Toxicológica, Facultad de Ciencias Químicas y Farmacéuticas, Universidad de Chile, 8380492 Santiago, Chile
[b] Instituto de Carboquímica, CSIC, c/Miguel Luesma, 4, 50018 Zaragoza, Spain

ARTICLE INFO

Article history:
Received 30 September 2011
Received in revised form 5 December 2011
Accepted 6 December 2011

Keywords:
Oxidized multi-walled nanotubes
Oxygen functional groups
Electrocatalysis
Hydrogen peroxide

ABSTRACT

The influence of chemical oxidation on the electrochemical behavior against hydrogen peroxide of long and short multi-walled carbon nanotubes (MWCNT) has been investigated. Different degrees of oxidation with a sulfo-nitric mixture and with nitric acid were used and a complete physical and oxygen functional group characterization was performed by Raman spectroscopy, Fourier transform infrared spectroscopy (FTIR), acid group titration, transmission and scanning electron microscopies (TEM/SEM), elemental analysis, thermogravimetric analysis (TGA), nitrogen adsorption isotherms and cyclic voltammetry. The results revealed that electrodes modified using pristine short CNT (*s-NC*) present higher amperometric response against hydrogen peroxide than that obtained using long CNT (*l-NC*), which correlates with the greater degree of packing observed for *l-NC* by SEM and the long and thin structures observed in *s-NC*. On the other hand, the chemical oxidation process increases slightly the sensitivity of resulting electrodes, in about 25%, for both *s-NC* and *l-NC* indicating that for hydrogen peroxide oxidation the metal catalyst impurities, that are removed in the oxidation process, are not as relevant in the electrocatalysis as the increase in the capacitance values observed in the oxidized CNTs. The presence of oxygen groups introduces (a) new sites for redox reaction (pseudocapacitance) and (b) strong polar sites that would adsorb water molecules favoring double-layer formation (double-layer capacitance).

1. Introduction

Metal-free heterogeneous catalysis has become a necessity for a sustainable chemistry. The metal-based catalysts has several disadvantages, including their high cost, low selectivity, poor durability, and detrimental environmental effects caused by catalyst residues and/or undesirable side-products [1].

In electrochemistry, carbon nanotubes (CNTs) are being used increasingly in applications that include cell components for batteries and fuel cells, supercapacitors and electrochemical biosensors [2,3]. Important advantages in electrochemistry have been claimed for CNTs over other carbon materials such as glassy carbon and highly oriented pyrolitic graphite (HOPG). These characteristics include a decrease in overpotentials, low capacitance in the pristine state (arising from the low density of states of CNTs) [4,5] and increase in peak currents, and thus lower detection limits, providing high sensitivity and selectivity in analytical sensing.

The exact origin of the electrocatalytic properties of CNTs had not been fully explained and there is significant debate about the fundamental electroactivity of CNTs [6,7]. A considerable body of the literature suggests that the CNT sidewall is inert and that edge-plane-graphite-like open ends and defect sites are responsible for the electron transfer activity observed. In contrast, studies of well-characterized single-walled nanotube (SWNT) modified electrodes, either as individual tubes or as two-dimensional networks, suggest sidewall activity [3].

Due to the interfacial nature of electrochemical processes, the CNT surface state is very important. The presence of surface charged groups such as oxygen functional groups, amorphous carbon or metal nanoparticles [8] is likely to affect the behavior of CNT-based electrodes.

The effect of CNT oxidative treatments on the electrochemical behavior of CNTs involving gas-phase [9,10], electrochemical [11] and liquid-phase [12] oxidations have been published. Reports relate the changes in physical and chemical properties of oxidized CNTs with electrochemical properties such as capacitance [13] and an change in the electroanalytical sensing properties of a CNT-modified electrode. Recently Kruusenberg et al. [14] concluded that the acid-treated CNT modified GC electrodes are less active

* Corresponding author. Tel.: +56 29782896; fax: +56 29782988.
E-mail address: sbollo@ciq.uchile.cl (S. Bollo).
[1] ISE member.

0013-4686/$ – see front matter © 2011 Elsevier Ltd. All rights reserved.
doi:10.1016/j.electacta.2011.12.043

catalysts for oxygen reduction than as-received CNTs which was explained by the absence of metal catalysts on the surface of purified CNTs.

As grown CNTs are multicomponent materials consisting of CNTs (single-walled or multi-walled), metal nanoparticles and more or less graphitized carbon phases, many groups have emphasized the need for CNT purification. Oxidative treatments are the most frequently used purification methods, among which the most common methods are nitric (HNO_3) and sulfuric (H_2SO_4) acid oxidation [15], oxygen [16], ozone oxidation [17] and plasma oxidation [18]. The use of acid purification processes produces side effects such as the cutting and opening of CNT ends, which causes defects in the CNT sp^2 structure that is functionalized with oxygen-containing groups, such as carboxylic acids, ketones and alcohols [19]. A number of systematic studies have been conducted regarding the effect of oxidative treatments on the chemical nature of the graphitic structure. In 1999, Figueiredo et al. [20] described that gas phase oxidation of the carbon mainly increases the concentration of hydroxyl and carbonyl surface groups, while oxidations in liquid phase particularly increase the concentration of carboxylic acids. Datsyuk et al. [21] evaluated the effect of oxidation on the structural integrity of MWCNTs through acid and basic agents. They concluded that the material treated with nitric acid under reflux conditions undergoes the highest degree of degradation, i.e., nanotube shortening and additional defects in the graphitic network. On the other hand, basic oxidative treatment led to the complete removal of amorphous carbon and metal oxide impurities, but the structural integrity was found to be intact. Also, they determined a clear increase in the oxygen content on the walls of CNTs for all treatments tested. The oxygen functionalities depend on the oxidation conditions and the overall amount of oxygen increase with the increasing power of the oxidation agents.

In accordance with the state of the art, this paper addresses the electrochemical characterization of MWCNT (long and short) after different degrees of oxidation with a sulfo-nitric mixture and with nitric acid and provides their final application against hydrogen peroxide oxidation. Hydrogen peroxide it is a redox marker of several biological processes and CNTs have demonstrated an important catalytic effect on their redox process [22,23].

2. Experimental methods

2.1. Materials

MWCNTs of two different lengths were used: short (1–5 μm long and 30 ± 15 nm diameter), referred to as *s-NC* and long (5–20 μm long and 30 ± 15 nm diameter) referred to as *l-NC*. Both types of CNTs were provided by NanoLab (USA).

Chitosan (CHI) of medium molecular weight (Cat. No. 44887-7) was obtained from Aldrich, glutaraldehyde (GTA) (25%, v/v, aqueous solution) was purchased from Baker and hydrogen peroxide (30%, v/v, aqueous solution) was purchased from Merck.

2.2. CNT functionalization

2.2.1. Mixture of 3 mol dm^{-3} nitric (HNO_3, 65%) and sulfuric (H_2SO_4, 96%) acids

Small quantities of *s-NC* and *l-NC* (<100 mg) were immersed in a 50 mL H_2SO_4/HNO_3 (3:1) solution in a round-bottomed glass flask. The mixtures were heated to ~110 °C and the experiment was considered to have started at the moment the first reflux drops appeared. A fraction of the CNTs was oxidized for 3 h, while another fraction was oxidized for 6 h. Finally, oxidized MWCNTs were filtered and washed thoroughly with deionized water until a neutral pH was reached, and then dried at 50 °C for 24 h.

Table 1
Codes of samples for short (*s-*) and long (*l-*) CNT after each oxidizing agent at different times.

Code	Oxidizing agent	Oxidation time (h)
NC	–	–
NCO3	H_2SO_4/HNO_3	3
NCO6	H_2SO_4/HNO_3	6
NCO7N	HNO_3	6

2.2.2. Concentrated 7 mol dm^{-3} nitric acid, HNO_3

250 mg of *l-NC* was added to 100 mL of HNO_3 aqueous solution and refluxed for 6 h. The suspension was filtered and washed with distilled water and dried under vacuum. The code of all the samples is presented in Table 1.

2.3. Characterization of functionalized CNTs

Pristine and functionalized MWCNT samples were characterized by several techniques. FTIR, Raman spectroscopy, elemental analysis, acid group determination and XPS were used to estimate the surface groups on the CNT before and after acid treatment. TGA provided information on the changes in thermal stability. Structure and morphology were studied by high-resolution transmission electron microscopy (HRTEM) and SEM. Nitrogen adsorption isotherms were used to investigate modifications in surface area density and porosity. Finally, cyclic voltammetry was used to determine the electrochemical behavior.

FTIR was carried out in a Bruker Vertex 70 spectrometer. All samples were prepared as pellets using KBr spectroscopic grade. Raman spectroscopy was performed using a Renishaw micro-Raman spectrometer, working with a 532 nm He–Ne laser beam; each spectrum was acquired using a 25× objective. All spectra were collected with accumulations of 10 s each one and the spectra were analyzed, base-line corrected and normalized with NGS LabSpec software. Elemental analysis was carried out with a Flash 1112 analyzer from Thermo Fisher Scientific. Oxygen determination was carried out separately in the same device; the pyrolisis gases were absorbed on carbon black, then separated and conducted to a thermal conductivity detector.

The total acidic sites were determined by titration with NaOH, and carboxylic acid groups were individually determined by titration with $NaHCO_3$ using a modification of a previously used titration method [24,25]. Neutralization with NaOH and $NaHCO_3$ was developed and the samples were then filtered and washed thoroughly until neutral pH was reached and ICP analysis was performed to determine the quantity of Na present.

X-ray photoelectron spectroscopy (XPS) was performed with an ESCAPlus Omicron. The analysis area was 1.75 mm × 2.75 mm and the beam energy was 150 W (10 kV, 15 mA).

Cyclic voltammograms were recorded using a CHI 900 potentiostat. A three-electrode cell was used with an Ag/AgCl/3 mol dm^{-3} NaCl (BAS) and a platinum wire as reference and auxiliary electrodes, respectively. The modified working electrode was prepared by polishing a glassy carbon electrode (GCE) with 0.3 μm and 0.05 μm alumina, and then was washed with abundant deionized water. The CNTs were dispersed at 1 mg mL^{-1} concentration with a phosphate buffer solution (PBS) pH 7.4 and 0.1 mol dm^{-3} NaCl by sonication for 15 min. The sonication procedure was repeated three times. CNT immobilization was performed by casting the GCE with 8 μL of the CNT dispersion. The optimum conditions were obtained by drying the dispersion dropped onto the GCE for 15 min at 50 °C in a stove. The resulting modified electrodes were called GCE/CNT. Thermal studies were carried out by means of TGA using a Setaram SETSYS Evolution 16/18 analyzer. The samples were scanned within the temperature range of 0–1500 °C at a

ramp rate of 5 °C min^{-1}. SEM and HRTEM samples were adsorbed onto Formvar/carbon coated-grids and negatively stained with 2% uranyl acetate. They were observed in a Jeol 1010 transmission electron microscope, and images were digitized with an SIS Megaview III Camera. The specific surface areas (SSA) of CNTs were determined by N_2 adsorption isotherm using a BET Micromeritics ASAP2020.

2.4. Electrochemical behavior of hydrogen peroxide

CNTs were dispersed in a 1.0% (w/v) CHI solution prepared in 1.0% (v/v) acetic acid solution by sonicating for 30 min with a final concentration of 1 mg mL^{-1}. Prior to surface modification, the GCE was cleaned by polishing with 0.3 and 0.05 μm alumina slurries for 1 min. The immobilization of CNTs was performed by casting the GCE with 8 μL of the CHI-CNT dispersion. Optimum conditions included drying the dispersion that was dropped onto the GCE for 15 min at 50 °C, followed by reaction with 3.0% (v/v) GTA for 2 s. The electrode was then washed by immersion in buffer solution for 10 s.

Amperometric measurements were conducted in a stirred 0.20 mol dm^{-3} phosphate buffer solution, pH 7.40, by applying the desired working potential and allowing the transient currents to decay to a steady-state value prior to the addition of the analyte and subsequent current monitoring. All measurements were performed at room temperature. The experiments were conducted in triplicate.

3. Results and discussion

3.1. Physical characterization

Morphological changes on *l-NC* and *s-NC* produced by the oxidative treatment and time were detected using scanning electron microscopy. As observed in Fig. 1A and B, *s-NC* show long and thin structures while *l-NC* show blocks, suggesting a greater degree of packing, i.e., *l-NC* present a more compact structure. Furthermore, no metallic impurities are observed.

After the oxidative treatment with sulfo-nitric mixture (Fig. 1C–F), the nanostructures do not seem to be harmed. In spite of the liquid media treatment, the images of treated samples do not show an important increase in the degree of packing, possibly owing to the increase in the repulsive electrostatic forces between CNTs as a consequence of the incorporation of oxygenated functions. The oxidized largest CNTs still seem to be more compact, resulting in a less homogeneous, and rougher and porous surface.

CNT structures and the effect of chemical treatment on them were also characterized by HRTEM (Fig. 1S, supporting information). HRTEM images show that the raw material contains CNTs with different internal diameters (3.76 and 6.32 nm), external diameters (9.13 and 19.26 nm) and number of layers (8 and 19). The presence of amorphous carbon on the edge of a pristine sample is also observed. After oxidation with the sulfo-nitric mixture for 3 and 6 h, there are some differences compared with the raw samples, the most important being that the treatment caused etching of graphene sheets and an increase in the amount of amorphous carbon on the sidewalls.

CNT surface chemistry is of paramount importance for electrochemical behavior. Thus, the specific surface areas (SSAs) were modeled using the multilayer adsorption model proposed by Brauner, Emmet and Teller (BET). The adsorption isotherms for all the samples are type-II according to the IUPAC classification [26] and a little hysteresis is observed (Fig. 2S). Additionally, it can be seen that there is an increase in the amount of nitrogen adsorption at low P/P_o indicating the presence of microporosities. The maximum nitrogen adsorption at $P/P_o \sim 1$ decreases as long as the sample is treated with the sulfo-nitric mixture and this decrease is greater when nitric acid is used (*s-NCO7N*) (insets Fig. 2S).

Table 2
Physical parameters obtained for raw and oxidized samples.

Sample	Adsorption isotherms		Raman spectroscopy
	S_{BET} (m^2 g^{-1})	$V_{Mesopore}$ (cm^3 g^{-1})	I_D/I_G
s-NC	298	0.731	1.02
s-NCO3	267	0.577	1.15
s-NCO6	266	0.556	1.33
s-NCO7N	256	0.644	1.39
l-NC	378	0.826	1.09
l-NCO3	380	0.685	1.35
l-NLO6	336	0.535	1.49

The determined values of S_{BET} are presented in Table 2. As can be seen, when the samples are oxidized, the BET surfaces decrease between 10.8 and 14.1%. In general the literature reports that oxidative treatments increase the BET surface areas [13,27] particularly in gas-phase oxidations [9]; however similar findings to ours have been described for double-walled NTs where the S_{BET} decreases by approximately 35% after nitric acid oxidation [12], while others report no significant changes after similar treatments [28], although no explanation is given.

One explanation for our results could be that nanotubes of different diameters and orientations interact by means of intermolecular forces to form aggregates that decrease the SSA. On the other hand, the samples oxidized with the sulfo-nitric mixture show a decrease in the mesopore volume as long as the time of oxidation increases, which indicates the formation of more compact aggregates. This is in agreement with the SEM images, where the oxidative treatment favors the formation of more compact bundles. Therefore, this process leaves fewer surfaces exposed for nitrogen adsorption.

In the Raman spectra of *l-NC*, oxidized at 0, 3 and 6 h (Fig. 3S.A) two bands are observed in the high-frequency region of the spectrum, exhibiting the CNT characteristics; the D band (~1350 cm^{-1}) is usually attributed to the presence of amorphous or disordered carbon and the G band (~1580 cm^{-1}) originates from in-plane tangential stretching of the C–C bonds in graphene sheets, indicating the presence of crystalline graphitic carbon in the CNTs. When the oxidative process was performed, the main change was the decrease in the G band. This change produced an increase in the ratio between D and G band intensities, noted as I_D/I_G, which is related to the degree of nanotube disorder. An increase in the I_D/I_G value corresponds to a higher proportion of sp^3 carbon, which is generally attributed to the presence of more structural defects. This behavior is also observed for the shortest samples but with lower intensity (Fig. 3S.B). The I_D/I_G values are presented in Table 2. At longer oxidation times and for the longest CNTs, the I_D/I_G value increases, this suggests the incorporation of more functional groups on the nanotubes.

The thermal degradation of the oxidized CNTs is greater than that of the raw *l-NC* sample. Below 150 °C, a lower weight loss (<2%) was observed for all samples, which corresponds to evaporation of the adsorbed water (Fig. 4S). Between 150 and 350 °C, the weight loss is mainly attributed to the CO_2 evolution of the carboxylic groups. The highest loss corresponds to *l-NCO7N* (9.7%), which seems to indicate a higher amount of functional groups present in this sample. This is in agreement with FTIR and elemental analysis results, as will be shown later. Thermal degradation from 350 to 500 °C may be attributed to the elimination of hydroxyl/ether functionalities attached to the CNT walls. Finally, at temperatures between 500 and 600 °C, the observed degradation corresponds to the decarboxylation of lactone and anhydrides, while above

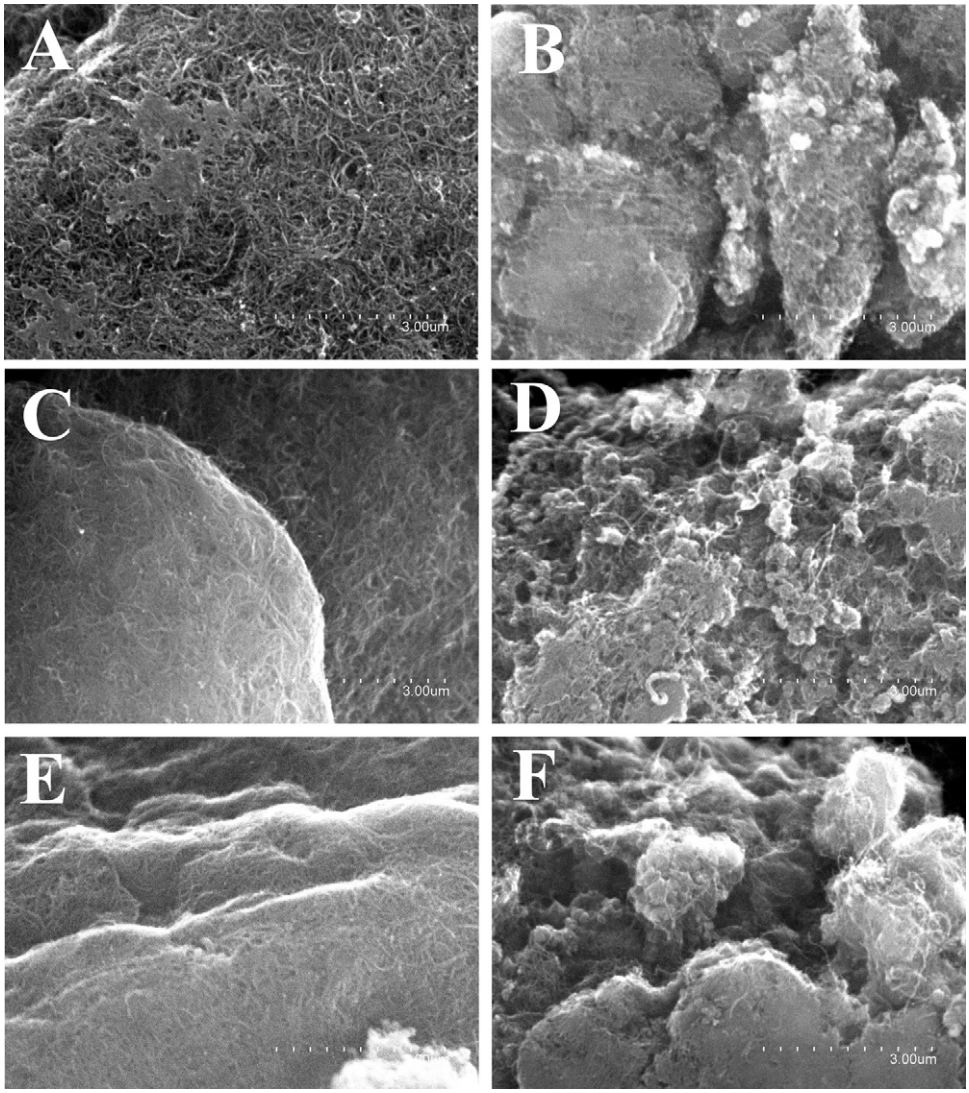

Fig. 1. SEM images of raw *s-NC* (A) and *l-NC* (B) MWNTs and after oxidizing with H_2SO_4/HNO_3 for 3 and 6 h. (C) *s-NCO3*, (D) *l-NCO3*, (E) *s-NCO6* and (F) *l-NCO6*.

600 °C, the weight loss could originate from phenols, ethers and carbonyls/quinones [20].

The sample with the greatest weight loss at all temperatures was *l-NCO7N* (>10%). This appears to be due to the different major functional groups it contains, compared with those introduced by the sulfo-nitric mixture. A similar situation was also observed in the case of the shortest samples derived from *s-NC*.

3.2. Chemical characterization

Elemental analysis was performed on raw (*s-NC*, *l-NC*) and oxidized samples, as shown in Table 1S. The percentage of oxygen in the samples shows that both raw *s-NC* and *l-NC* samples have oxygenated functional groups. When the samples were treated with the sulfo-nitric mixture, the oxygen content increased and there was a correlation between the time of oxidation and the oxygen percentage. On the other hand, the oxygen percentage is higher for those treated with 7.0 mol dm^{-3} HNO_3 (*s-NCO7N*, *l-NCO7N*). However, these samples also show an important increase in the nitrogen percentage, which suggests that part of the oxygen increase could be due to the ability of nitric acid to provide electrophilic nitronium ions capable of nitrating aromatic rings [29,30].

Infrared spectroscopy was used to characterize the samples in order to identify the CNT surface functional groups (Fig. 5S). All spectra present the 1580 cm^{-1} peak corresponding to the aromatic C=C structural vibrations. This band shifts to higher frequencies (1575/1580/1582 cm^{-1}) when the oxidation progresses and it is enhanced owing to the increasing density of surface oxygen [30]. Additionally, the FTIR spectra for all samples show absorption bands at 3430 cm^{-1} (O—H from hydroxyl or carboxyl groups and phenol groups), 2916 and 2848 cm^{-1} (C—H) and a broad band between 1050 and 1300 cm^{-1} (C—O from ethers, alcohols, anhydrides, lactones or carboxylic acids). All these bands present in raw MWCNTs indicates the presence of some oxygenated functional groups introduced during the synthesis process.

After the MWCNT acid treatment, there was an increase in the bands around 3400 cm^{-1} and 1100 cm^{-1} and a new band developed at about 1700 cm^{-1}, corresponding to carboxylic acid groups that show absorption between 1690 and 1730 cm^{-1}. The intensity of this band, relative to the 1560 cm^{-1} band, increases when the oxidation time with the sulfo-nitric acid treatment is increased and with the nitric acid treatment. After oxidative treatments, all bands related to oxygen groups increase their intensity in the 1050–1300 cm^{-1} region. The oxidized samples also show

Table 3
Total acid groups and carboxylic groups after the oxidative treatments.

Sample	%Na (NaOH)	%Na ($NaHCO_3$)
s-NC	0.57	0.51
s-NCO3	1.63	1.55
s-NCO6	1.92	1.91
s-NCO7N	1.96	1.39
l-NC	0.66	0.42
l-NCO3	2.35	1.83
l-NCO6	2.87	2.39
l-NCO7N	3.35	3.38

increased intensity in the 1600–1800 cm^{-1} band, corresponding to quinones (1550–1600 cm^{-1}), lactones (1675–1790 cm^{-1}) and anhydrides (1790–1880 cm^{-1}).

In the 1600–1800 cm^{-1} region, a shoulder appears in *l-NCO3* samples at about 1630 cm^{-1} that can be assigned to the quinone groups that become more prominent in sample *l-NCO6*, which increases considerably in sample *l-NCO7N*. The nitric acid treatment introduces higher amounts of quinone relative to carboxylic groups than the sulfo-nitric mixture treatment. This behavior is also observed for *s-NC* but with lower intensity.

The nitro group (—NO_2) group is isoelectronic with the carboxilate group (—CO_2) and both provide very similar spectra [31], which makes identification by IR difficult. Some contributions from these groups are probably present, as can be inferred by the elemental analysis.

The quantification of acidic oxygenated groups introduced by oxidation was employed modifying a previously published titration method [24,25]. Na adsorption on the as-grown nanotubes was also quantified in order to determine the signal not coming from the neutralization of newly formed acidic groups. It is generally accepted that the total acidic sites – carboxylic, lactonic and phenolic – can be determined by titration with NaOH, while most acid groups – carboxylic – can be determined by titration with $NaHCO_3$ ($pK = 6.37$) [29].

The number of groups neutralized with $NaHCO_3$ and NaOH is shown in Table 3. *l-NC* shows a higher amount of acidic groups than *s-NC*. Likewise, it has been observed that oxidation with the sulfo-nitric mixture is time dependent, and oxidation with nitric acid introduces a higher number of acid groups in *l-NC* than sulfo-nitric oxidation. This is not the case of *s-NC*, where the maximum amount of acidic groups with the highest acidity corresponds to sample *s-NCO6*. It is known that oxidative processes involving sp^2 carbon atoms start with the creation of an alcohol group, followed by a ketone group before finally yielding a carboxylic group [25,32]. Taking into account the progress in the oxidative process, the higher degree of *l-NC* oxidation could explain the higher content in acidic groups compared with *s-NC*.

With regard to the type of acidic oxygenated groups, several studies [33–35] have demonstrated that a distribution of oxygenated groups is introduced by oxidation, but only those with pK_a between 3 and 10 can be determined. Groups below or over this range will not be detected by titration experimentally, so the results in Table 3 could underestimate the amount of acid groups.

Additionally, in organic chemistry it is known that the ortho-positioned groups in an aromatic ring bonded to —COOH increase the acidity of those acids. For example, ortho NO_2 groups in benzoic acid result in a pK_a decrease from 4.19 to 2.16 [36]. The elemental analysis shows that nitro groups, whether intercalated or bonded to the aromatic ring, are present after our oxidative process with nitric acid, which could lead to titration results different from those expected in nitric acid-treated samples.

Ending with the chemical characterization X-Ray Photoelectron Spectroscopy was used to identify the different oxygen functionalities incorporated on the MWCNT structure. The interpretation of O 1s spectrum was done according to the following sub-band classification [20,37]:

- Group I at 531.1 eV: carbonyl/quinone groups (C═O).
- Group II at 532.3 eV: alcohol/phenol (—OH), ether (—O—) groups, as well as the C═O bond from anhydride/lactone groups O—(C═O).
- Group III at 533.3 eV: anhydride/lactone groups O═(C—O).
- Group IV at 534.2 eV: carboxylic —COOR groups.

The high-resolution O 1s spectrum of the *l-NC* sample shows a very low intensity (Fig. 2) owing to its low oxygen content. The band is centered at 532.2 eV, which is the position of alcohol, phenol, and ether groups. This is consistent with the IR spectrum absorption bands around 3400 cm^{-1} and 1050–1300 cm^{-1} region. According to TGA results, it must be assumed that the *l-NC* sample has certain amounts of carbonyl and anhydride groups, although their XPS signal would be embedded into the main alcohol/ether band.

The spectrum of sample *l-NCO3* shows an intense band centered at 532.4 eV with a shoulder at 529.9 eV. The sub-bands bands at 532.3 and 533.3 eV indicate a high content in anhydride groups.

Alternatively, the combination of both bands could be due to certain amounts of alcohol/phenol and lactone groups. The sub-band at 534.2 eV confirms the formation of a few carboxylic acid groups. The sub-band at around 531.1 eV is due to carbonyl/quinone groups. The sub-band at 529.9 eV indicates the formation of iron oxide [21].

l-NCO6 sample spectrum has a main band at 533.0 eV with a shoulder between 531 and 532 eV. The sub-band of carboxylic groups at 534.2 eV increases substantially. Lactone, anhydride, hydroxyl and carbonyl group bands can be also found in the spectrum. *l-NCO3* and *l-NCO6* XPS data are in agreement with the development of the 1708 cm^{-1} IR bands corresponding to carboxylic acid groups and the increase in intensity of the C═O stretching at 1120–1200 cm^{-1} and C—O in ethers (1000–1300 cm^{-1}), lactones (1160–1370 cm^{-1}) and anhydrides (980–1300 cm^{-1}) [38].

l-NCO7N spectrum presents a wide band centered at around 532.3 eV. The content in carboxylic groups is lower than in the *l-NCO6* sample. The sub-band at 533.3 eV indicates an increase in the amount of lactone groups and the sub-band at 531.1 eV increases, this correlates with the increase of the quinone band (1650 cm^{-1}) in the IR absorption spectra. Anhydride, hydroxyl and carbonyl groups are also present on *l-NCO7N* surfaces.

According the titration data the number of groups with higher acidity neutralized with $NaHCO_3$ increases by increase the oxidation time for both short and long CNTs that is consistent with the increase of COOR groups in XPS data. After oxidation with nitric acid the number of groups determined by titration with $NaHCO_3$ is lower than with sulfo-nitric mixture for short and long CNTs as determined by XPS. However according titration data the number of acid groups in long CNTs is higher in nitric acid treated samples. As mentioned before this seems to indicate that the titration data for this sample could be overestimated due to the presence of NO_2 ortho positioned to carboxylic groups.

C 1s XPS spectra for the oxidized l-NC samples shows that the intensity between 285 and 290 eV increases with the degree of oxidation (Fig. 6S). In agreement with previous reports [39,40], deconvolution of the C 1s region of the spectra leads to misleading and ambiguous results in terms of the calculated distribution of oxygen-containing functional groups owing to the proximity of the binding energies associated with different oxygen-containing functional groups.

Pristine MWCNTs have a low iron content (0.94 wt.%) and a low intensity band appears in the XPS 2p spectrum (Fig. 7S) at 707.5 eV. According to the assignations reported by Yang and Sacher [41], this

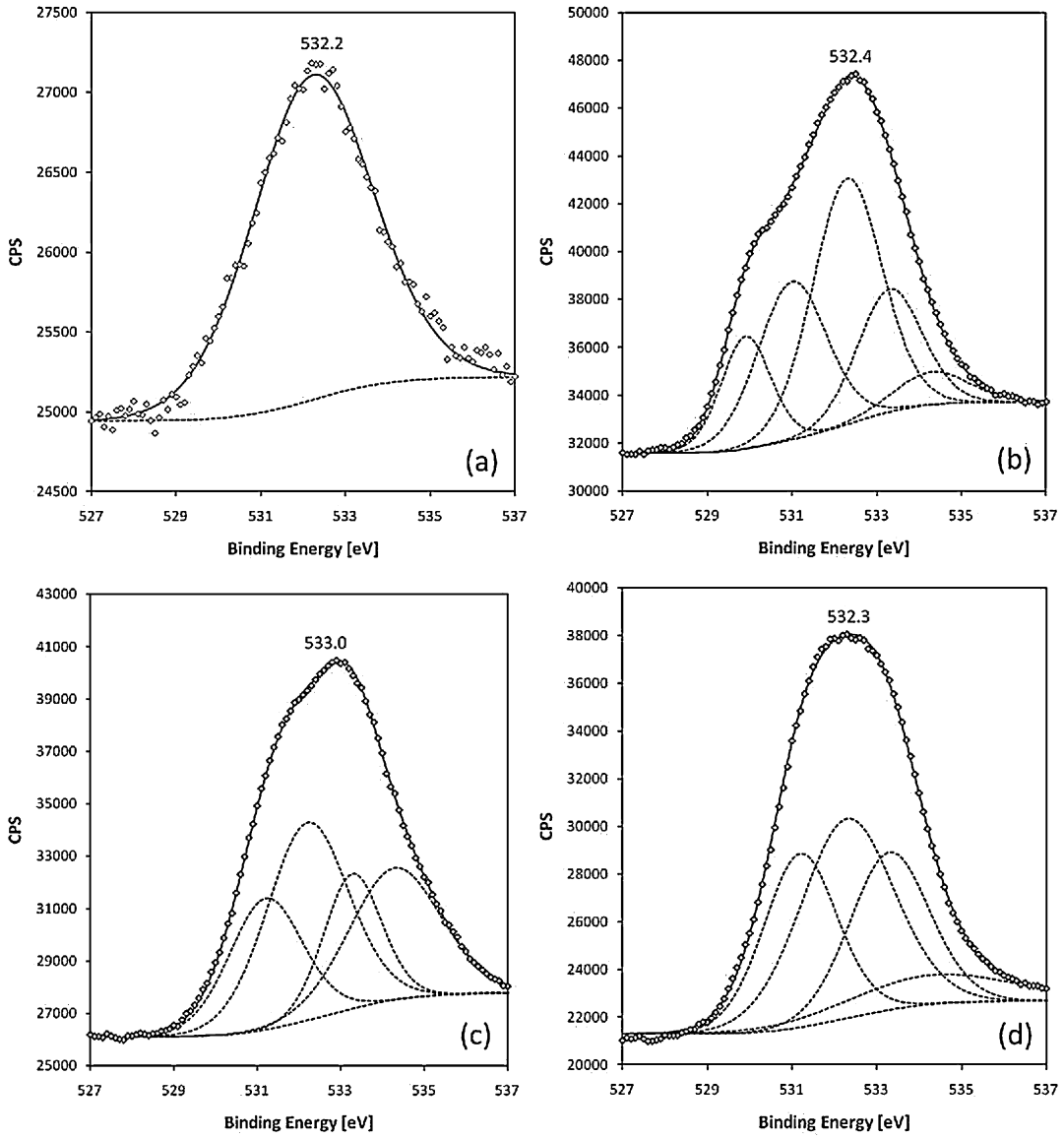

Fig. 2. High-resolution O 1s spectra for: *l-NC* (A), *l-NCO3* (B), *l-NCO6* (C), and *l-NCO7N* (D).

peak could be due to Fe^0. After sulfo-nitric treatment, this band almost disappears in sample *l-NCO3* and a new band appears at 710.2 eV that could correspond to Fe_3O_4. Poulin et al. [42] attributed the XPS peak position at 709.6 eV to Fe^{II} octahedral and at 710.2 eV to Fe^{III} octahedral. The developing of this band agrees with the presence of the sub-band at 529.9 eV in the O 2p XPS spectrum that indicates the formation of iron oxide.

After more severe acid treatments in samples *l-NCO6* and *l-NCO7N*, the signal around 710 eV in the Fe 2p XPS spectrum disappears indicating that the iron oxide has been removed, particularly in sample *l-NCO7N*.

Fig. 3 shows a histogram of the distribution of oxygen groups in *l-NC* and *s-NC* pristine and oxidized samples. Given that XPS is only surface sensitive, the distribution of the total oxygen determined directly by elemental analysis according to the proportion given by XPS is depicted. The oxygen corresponding to the iron oxide has been discounted in this distribution. The analysis of the data indicates that both treatments, nitric and sulfo-nitric acid, progressively increase the amount of carbonyl/quinone groups (C═O) and group II oxygenated groups corresponding to alcohol/phenol (—OH) and ether (—O—) groups, as well as the C═O bond from anhydride/lactone groups O—(C═O). The content of these groups is greatest with nitric acid treatment, and the same behavior is observed for both *l-NC* and *s-NC* nanotubes. Conversely group IV, corresponding to carboxylic/carboxylate groups, increases when the sulfo-nitric treatment time is increased from 3 to 6 h but is lower in samples treated with nitric acid. Both *l-NCO6* and *s-NCO6* samples contain the maximum amount of carboxylic groups. Group III, corresponding to anhydride/lactone groups O═(C—O), shows a different tendency for *l-NC* and *s-NC*. These groups in *l-NC* samples increase by passing from *l-NCO3* to *l-NCO6* and *l-NCO7N*. Nevertheless, the number of these groups in *s-NC* does not increase with nitric acid treatment and reaches a plateau. This could be explained owing to the fact that quinone, lactone and anhydride moieties are generated in greater quantity than carboxylic groups with such oxidative treatment.

On the other hand, deconvolution of N 1s XPS (Fig. 8S) results in two peaks at 400.5 and 405.7 eV that can be attributed to nitrogen atoms bound to carbon (N—C) and to oxygen (N—O), respectively, confirming the incorporation of nitrogen into the CNT structure.

It was expected that as short CNTs have more tips and consequently more defects, more reaction sites will be oxidized. However

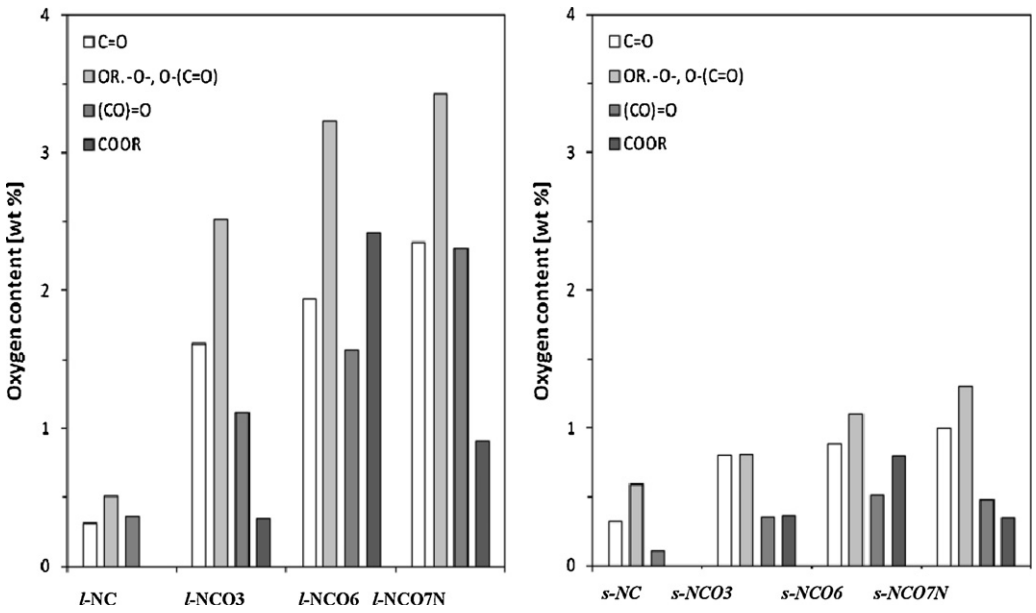

Fig. 3. Quantification of the oxygen group contents from O 1s XPS spectra.

our study shows higher degree of oxidation in long CNTs. According to elemental analysis the amount of oxygen in long CNT samples is higher (for both 3 and 6 h of treatment) and this is consistent with the higher I_D/I_G value of long CNT after oxidative treatment. Other data that support the higher oxidation of long CNT are TGA data showing higher weight loss in long CNTs, and higher number of oxygen functional groups as determined by XPS and titration with NaOH. One possible explanation would be that in the conditions used for the oxidative treatment, the side wall functionalization is more important than tip functionalization.

3.3. Electrochemical characterization

CNT film-modified glassy carbon electrodes (GCE/CNT) are generated using non-oxidized CNTs (*s-NC*) reveal no electrochemical signal (Fig. 4A), indicating that the small amount of oxygenated functional groups observed with XPS (alcohol/phenol and ether) are not electrochemically active, nor is the iron present in the pristine nanotubes. The CV curves are rectangular with good symmetry for all the electrodes prepared, showing typical electric double layer behavior [43].

When GCE/CNT are generated using oxidized samples, a redox couple is observed by cyclic voltammetry in PBS solution at pH 7.4 (Fig. 4A dashed lines), in a similar way to that previously described [14,44]. The redox couple corresponds to the carboxylic acid group incorporated in the CNT structure, but we estimated that other oxygenated groups, such as quinone, contribute because they are also electroactive [3].

The electrodes modified with sulfo-nitric oxidized CNT revealed an increase in the current intensities as the oxidation time increases (Fig. 4B) and there is a correlation with the incorporated oxygen content determined by elemental analysis (wt%O). Thus, we can corroborate that higher oxidation time leads to higher current due to a high incorporation of carboxylic electroactive groups. Accordingly, it would be possible to predict the oxygen content by performing cyclic voltammetry, creating the opportunity for a new application of electrochemistry in CNT characterization. On the other hand, the same Fig. 4B shows a comparison between the oxidative protocols, sulfo-nitric mixture (*s-NCO6*) and nitric acid (*s-NCO7N*) being possible to observe that there is an increase in the current intensity when the electrode was modified using *s-NCO7N* but the oxygen content remains constant. These results corroborate that the oxygen groups incorporated with nitric acid are different than that incorporate when sulfo-nitric mixture is used. The increase in the current intensity without the increase in the oxygen

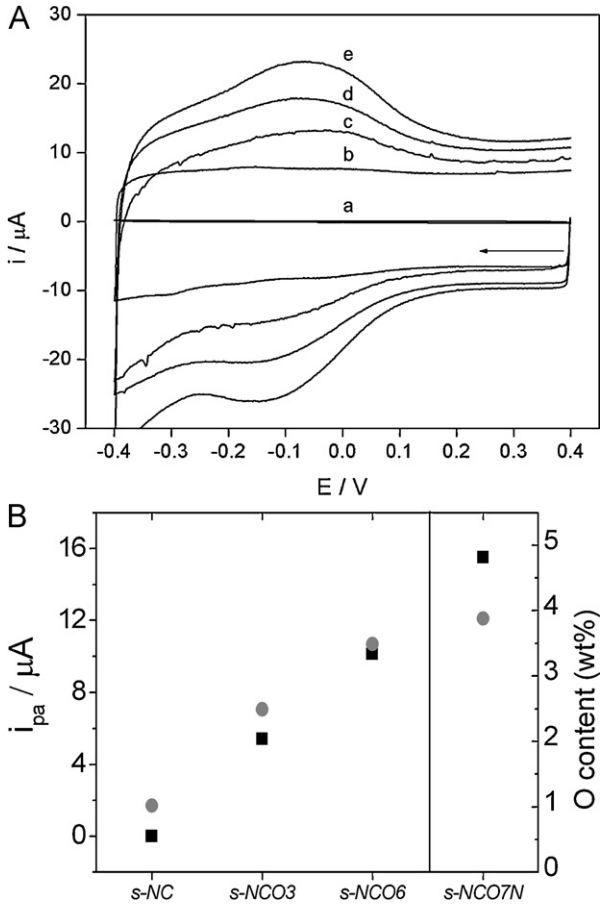

Fig. 4. (A) Cyclic voltammograms of *s-NC* films onto GCE. The electrochemical response corresponds to the redox couple of carboxylic acids: GCE (a), *s-NC* (b), *s-NCO3* (c), *s-NCO6* (d), *s-NCO7N* (e). (B) Relation of the cyclic voltammetric current intensities (■) and the oxygen content (wt%) (●) with chemical treatment of MWCNTs.

content is concordant with more quinones than carboxylic groups in s-*NCO7N* which suffers a two electron redox process and then more current intensity than the one electron process of carboxylic acids.

Also, the longest CNT shows a higher degree of oxidation and higher current values, indicating that more electroactive groups are incorporated as was determined previously by Raman Spectroscopy and Elemental Analysis.

The HNO_3 treatment leads to a higher degree of oxidation and the introduction of an electroactive group, according to XPS data.

Nevertheless, the number of carboxylic groups is the highest for the 6-h sulfo-nitric treatment, indicating that in addition to the carboxylic groups, higher amounts of quinone, lactone and anhydride groups are being introduced with nitric acid treatment.

Analyzing the reversibility of the redox process oxidized *s-NC* samples show lower ΔE_P values than oxidized *l-NC* samples (100 vs. 140 mV, respectively), indicating that the electrochemical process occurs with a faster electron transfer rate on *s-NC*. Finally, no significant changes in the electron transfer rate were observed when the oxidation time was increased since the corresponding ΔE_P values did not change in a significant way.

The CNT-modified electrodes using short (*s-NC*, *s-NCO3* and *s-NCO6*) and long (*l-NC*, *l-NCO3* and *l-NCO6*) CNTs were also characterized by cyclic voltammetry in 0.2 mol dm^{-3} PBS pH 7.4, determining the capacitance values as reflect of the electroactive area of each electrode. When pristine CNTs are used to modify the electrodes, the resulting capacitances are similar, with values of 310 and 332 μF for *s-NC* and *l-NC*, respectively. After 6 h of oxidation, the capacitance values increase to 394 and 890 μF for *s-NCO6* and *l-NCO6*, respectively, i.e., there is a correlation with the amount of oxygen function incorporated and the resulting capacitance when the sulfo-nitric treatment is used. On the other hand, when CNTs were oxidized with nitric acid, the resulting capacities are 432 and 653 μF for *s-NCO7N* and *l-NLO7N*, respectively. The increased values would imply an increase in double-layer capacitance and also in pseudocapacitance as results of newly incorporated electroactive groups. The increase in double-layer capacitance due to functionalization (i.e., oxidation) can be attributed to an enhanced accessibility to hydrophilic carbon coverage in aqueous electrolyte.

Previously performed BET analysis showed that the oxidation process produces a slight reduction in the surface area and mesoporosity, implying less area available for double-layer formation. However, according to Hsieh et al. [45], this postulation is not completely true because not all carbon surfaces are electrochemically active, i.e., surface heterogeneity. Thus, the capacitance enhancement can be attributed to an increase in active coverage, and, therefore, the double-layer capacitance is directly proportional to the surface freely accessible to the electrolytes rather than the SSA obtained by the Brunauer–Emmett–Teller (BET) method [46].

3.4. Electrochemical behavior of hydrogen peroxide on CNTs modified electrodes

No significant change respect to GCE was observed for hydrogen peroxide reduction using CNT and oxidized CNT. However, a clear catalytic effect of CNTs on the oxidation of hydrogen peroxide was observed. Fig. 5 shows the voltammetric response obtained with GCE, GCE/CHI-*s-NC* and GCE/CHI-*l-NC*. Compared with the GCE, CNT-modified electrodes showed a decrease in the overvoltage for the oxidation of hydrogen peroxide by about 200 mV (700 mV for GCE and 500 mV for the *s-NC* and *l-NC* modified GCEs). Furthermore, there was an increase in the current intensities at potential higher than 600 mV.

From the amperometric hydrogen peroxide concentration study performed at 700 mV (Fig. 5 inset), higher currents were obtained with *s-NC* than *l-NC*, by about 200%. The lower sensitivity observed

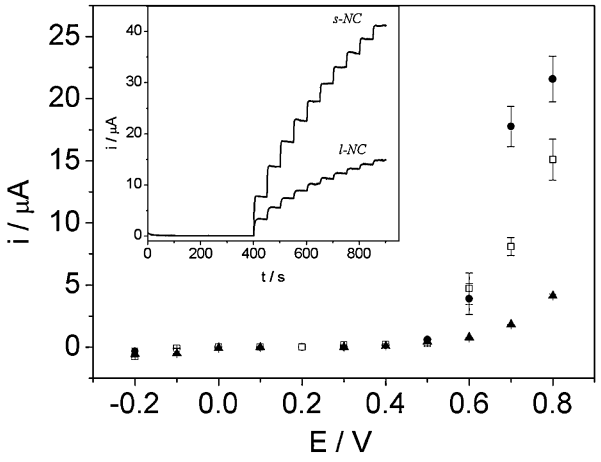

Fig. 5. Effect of the length of pristine CNT on the electrochemical response of 0.4 mol dm^{-3} hydrogen peroxide solution. Hydrodynamic voltammetry at GCE (▲), GCE/CHI-*l-NC* (□) and GCE/CHI-*s-NC* (●). The experiments were conducted in triplicate. Inset: amperometric response at 0.700 vs. (Ag/AgCl/3 mol dm^{-3} NaCl)/V.

with *l-NC* could be due their greater degree of packing, as was determined by SEM, i.e., *l-NC* are more compact while *s-NCs* show long and thin structures.

When the electrochemical behavior of hydrogen peroxide was tested using oxidized CNTs, the hydrodynamic voltammograms revealed no significant changes in the response between *s-NC*, *s-NCO3* and *s-NCO6* (Fig. 6). Only at 800 mV there was a significant increase in the observed current for *s-NCO6*. Indeed, from the amperometric hydrogen peroxide study performed at 700 mV (inset Fig. 6), similar calibration curves were obtained with electrodes modified with *s-NCO3* and *s-NCO6* samples, and a 25% increase in the response with respect to the GCEs modified with pristine CNTs was obtained. The same behavior was observed for long CNTs. Consequently it is possible to conclude that the sensing properties of CNT-modified electrodes against hydrogen peroxide are strongly dependent on the length of the nanotube more than the oxidation. An explanation could be related to the size of hydrogen peroxide which permits a fast diffusion through the double layer to easily reach the surface of the CNTs, allowing electron transfer to occur. On the other hand, our results show that although the oxidation of the CNT does not improve dramatically the electrochemical

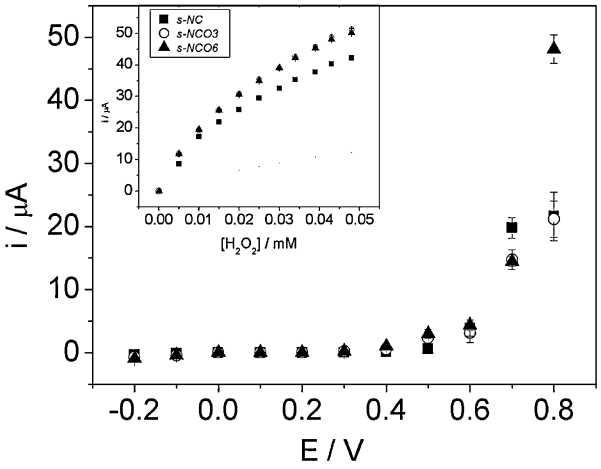

Fig. 6. Effect of the oxidation time on short CNTs with regard to the hydrodynamic electrochemical response of hydrogen peroxide solution. *s-NC* (■), *s-NCO3* (○) and *s-NCO6* (▲). Inset: calibration curves obtained at 0.700 vs. (Ag/AgCl/3 mol dm^{-3} NaCl)/V from successive additions of hydrogen peroxide. The experiments were conducted in triplicate.

response of modified electrodes, either there is a loss of sensitivity as has been reported for oxygen reduction recently [14].

4. Conclusions

The amount and type of oxygenated functional groups incorporated onto a CNT surface are strongly dependent on the reaction media and treatment time. Specific area and mesopore volume decrease with the treatments probably due to the CNTs become more compacted. SEM and Raman spectra showed that the integrity of the nanotube patterns was not damaged substantially by the acid treatment. With regard to the degree of oxidation, nitric acid treatment introduces a higher amount of total acidic groups (as determined by NaOH) than sulfo-nitric treatment (6 h). Infrared spectra and XPS indicate that nitric acid treatment leads to higher amounts of quinone, lactone and anhydride groups, whereas the sulfo-nitric mixture introduces higher amounts of carboxylic groups.

With regard to the electrochemical behavior, when the electrodes are modified with non-oxidized CNTs (*s-NC* and *l-NC*), no signal is observed, indicating that the small amount of oxygenated functional groups ($\approx$1% O_2) mainly phenol, alcohol and ether existing in the pristine nanotubes are not electroactive, nor is the iron present in the pristine nanotubes.

The oxidized CNT-modified electrodes show a clear difference in current intensities which correlate with the incorporated oxygen content. Likewise, the longest CNT shows a higher degree of oxidation and higher current values, indicating that more groups are incorporated, possibly owing to its higher S_{BET}. Oxidized *s-NC* shows lower ΔE_P than *l-NC*, indicating a faster electron transfer rate. Oxygen incorporation to CNTs leads to higher capacitance, i.e., higher electroactive surface, which can be attributed to an enhanced accessibility to hydrophilic carbon coverage in aqueous electrolyte.

In concordance, the electrochemical performance of oxidized CNT is strongly determined by the chemical characteristic of the CNT surface rather than the surface morphology.

Acknowledgements

We thank Dr. M. Campos Villete and Dr. A. Aliaga (Facultad de Ciencias, Universidad de Chile) for conducting the Raman spectroscopy experiments. Financial support from the Fondecyt-CHILE (Grant 1080526), CSIC 200480E481 Intramural Project and CSIC/CONICYT 2009CL0057 project (2010–2011) are gratefully acknowledged. P.C. acknowledges CONICYT scholarships for PhD studies in Chile, PhD scholarship support and PhD fellowship stay abroad (BECAS-CHILE).

Appendix A. Supplementary data

Supplementary data associated with this article can be found, in the online version, at doi:10.1016/j.electacta.2011.12.043.

References

[1] D. Yu, E. Nagelli, F. Du, L. Dai, The Journal of Physical Chemistry Letters 1 (2010) 2165.
[2] J. Wang, Electroanalysis 17 (2005) 7.
[3] X.B. Ji, R.O. Kadara, J. Krussma, Q.Y. Chen, C.E. Banks, Electroanalysis 22 (2010) 7.
[4] R.L. McCreery, Chemical Reviews 108 (2008) 2646.
[5] I. Heller, J. Kong, K.A. Williams, C. Dekker, S.G. Lemay, Journal of the American Chemical Society 128 (2006) 7353.
[6] C.E. Banks, R.G. Compton, Analyst 131 (2006) 15.
[7] I. Dumitrescu, P.R. Unwin, J.V. Macpherson, Chemical Communications (2009) 6886.
[8] C.E. Banks, A. Crossley, C. Salter, S.J. Wilkins, R.G. Compton, Angewandte Chemie-International Edition 45 (2006) 2533.
[9] M.-K. Seo, S.-J. Park, Current Applied Physics 10 (2010) 241.
[10] C.-T. Hsieh, W.-Y. Chen, Y.-S. Cheng, Electrochimica Acta 55 (2010) 5294.
[11] J.-S. Ye, X. Liu, H.F. Cui, W.-D. Zhang, F.-S. Sheu, T.M. Lim, Electrochemistry Communications 7 (2005) 249.
[12] I.Y. Jang, H. Muramatsu, K.C. Park, Y.J. Kim, M. Endo, Electrochemistry Communications 11 (2009) 719.
[13] C. Li, D. Wang, T. Liang, X. Wang, L. Ji, Materials Letters 58 (2004) 3774.
[14] I. Kruusenberg, N. Alexeyeva, K. Tammeveski, J. Kozlova, L. Matisen, V. Sammelselg, J. Solla-Gullón, J.M. Feliu, Carbon 49 (2011) 4031.
[15] J.G. Wiltshire, A.N. Khlobystov, L.J. Li, S.G. Lyapin, G.A.D. Briggs, R.J. Nicholas, Chemical Physics Letters 386 (2004) 239.
[16] A. Kuznetsova, I. Popova, J.T. Yates, M.J. Bronikowski, C.B. Huffman, J. Liu, R.E. Smalley, H.H. Hwu, J.G.G. Chen, Journal of the American Chemical Society 123 (2001) 10699.
[17] J.M. Simmons, B.M. Nichols, S.E. Baker, M.S. Marcus, O.M. Castellini, C.S. Lee, R.J. Hamers, M.A. Eriksson, Journal of Physical Chemistry B 110 (2006) 7113.
[18] C.L. Chen, B. Liang, A. Ogino, X.K. Wang, M. Nagatsu, Journal of Physical Chemistry C 113 (2009) 7659.
[19] D.B. Mawhinney, V. Naumenko, A. Kuznetsova, J.T. Yates, J. Liu, R.E. Smalley, Chemical Physics Letters 324 (2000) 213.
[20] J.L. Figueiredo, M.F.R. Pereira, M.M.A. Freitas, J.J.M. Orfao, Carbon 37 (1999) 1379.
[21] V. Datsyuk, M. Kalyva, K. Papagelis, J. Parthenios, D. Tasis, A. Siokou, I. Kallitsis, C. Galiotis, Carbon 46 (2008) 833.
[22] J. Kruusma, V. Sammelselg, C.E. Banks, Electrochemistry Communications 10 (2008) 1872.
[23] M.D. Rubianes, G.A. Rivas, Electrochemistry Communications 9 (2007) 480.
[24] H. Hu, P. Bhowmik, B. Zhao, M.A. Hamon, M.E. Itkis, R.C. Haddon, Chemical Physics Letters 345 (2001) 25.
[25] A.B. Gonzalez-Guerrero, E. Mendoza, E. Pellicer, F. Alsina, C. Fernandez-Sanchez, L.M. Lechuga, Chemical Physics Letters 462 (2008) 256.
[26] K.S.W. Sing, Pure and Applied Chemistry 57 (1985) 603.
[27] G. Wang, Y. Ling, F. Qian, X. Yang, X.-X. Liu, Y. Li, Journal of Power Sources 196 (2011) 5209.
[28] X.L. Chen, W.S. Li, C.L. Tan, W. Li, Y.Z. Wu, Journal of Power Sources 184 (2008) 668.
[29] I.I. Salame, T.J. Bandosz, Journal of Colloid and Interface Science 240 (2001) 252.
[30] C. Bower, A. Kleinhammes, Y. Wu, O. Zhou, Chemical Physics Letters 288 (1998) 481.
[31] J. Coates, Interpretation of Infrared Spectra, A Practical Approach, John Wiley & Sons Ltd, 2000.
[32] T.W.G. Solomons, J.E. Fernandez, Organic Chemistry, 5th ed., Wiley, New York, 1992.
[33] N. Briceno, M. Guzman, J. Diaz, Revista Colombiana de Química 36 (2007) 121.
[34] T.J. Bandosz, B. Buczek, T. Grzybek, J. Jagiello, Fuel 76 (1997) 1409–1416.
[35] A. Contescu, C. Contescu, K. Putyera, J.A. Schwarz, Carbon 35 (1997) 83.
[36] R.C. Weast, CRC Handbook of Chemistry and Physics, 1st Student ed., CRC Press, Boca Raton, FL, 1988.
[37] U. Zielke, K.J. Huttinger, W.P. Hoffman, Carbon 34 (1996) 983.
[38] P.E. Fanning, M.A. Vannice, Carbon 31 (1993) 721.
[39] K.A. Wepasnick, B.A. Smith, K.E. Schrote, H.K. Wilson, S.R. Diegelmann, D.H. Fairbrother, Carbon 49 (2011) 24.
[40] A.T. Masheter, L. Xiao, G.G. Wildgoose, A. Crossley, H.J.C. John, R.G. Compton, Journal of Materials Chemistry 17 (2007) 3515.
[41] D.Q. Yang, E. Sacher, Journal of Physical Chemistry C 113 (2009) 6418.
[42] S. Poulin, R. Franca, L. Moreau-Belanger, E. Sacher, Journal of Physical Chemistry C 114 (2010) 10711.
[43] K.H. An, K.K. Jeon, J.K. Heo, S.C. Lim, D.J. Bae, Y.H. Lee, Journal of the Electrochemical Society 149 (2002) A1058.
[44] H. Luo, Z. Shi, N. Li, Z. Gu, Q. Zhuang, Analytical Chemistry 73 (2001) 915.
[45] C.-T. Hsieh, H. Teng, W.-Y. Chen, Y.-S. Cheng, Carbon 48 (2010) 4219.
[46] H.-Q. Li, J.-Y. Luo, X.-F. Zhou, C.-Z. Yu, Y.-Y. Xia, Journal of The Electrochemistry Society 154 (2007) A731.